Test-particle drifts in traveling waves with cyclotron frequencies

Rikizo Hatakeyama, Naoyuki Sato,* and Noriyoshi Sato
Department of Electronic Engineering, Tohoku University, Sendai 980-77, Japan
(Received 14 June 1995)

When a test particle moves in the field of a traveling wave with the cyclotron frequency, a particle-acceleration difference is found to appear between the first half-cycle of the Larmor motion, during which the particle has a velocity component in the direction of the wave propagation, and the second half-cycle, during which it has a velocity component in the opposite direction. This asymmetric acceleration modifies the cyclotron-resonance trajectory, yielding the physical origin of the particle drift perpendicular both to the wave propagation and background magnetic-field lines. A perturbation method in the orbit theory sucessfully gives analytic expressions for and numerical calculations demonstrate the drift generation. The result is applicable to particle-flux control of magnetized plasmas.

PACS number(s): 52.65.Cc, 52.35.Fp, 52.35.Hr, 52.50.Gj

I. INTRODUCTION

The application of radio-frequency (RF) fields in the cyclotron range of frequencies has been one of the most used and successful methods in plasma production [1], heating [2], stabilization [3], and current drive [4]. In order to efficiently perform such works main efforts have been directed towards controlling spatial profiles of the excited waves, externally determining wave numbers that are parallel and perpendicular to background magnetic-field lines or preferred directions of wave propagation, and so on. When we focus our attention on phenomena that are perpendicular to the background magnetic field in these experimental procedures, it is expected that power absorption of charged particles from RF fields near the cyclotron frequencies is accompanied by perpendicular momentum transfer to them, which may in turn give effects on plasma transport across the magnetic field. From an experimental point of view, however, much attention has not been paid to this kind of RF-induced transport, although methods of flux control by low-frequency electromagnetic fields were proposed to improve plasma confinement [5] or kinetic theories on the RF-induced fluxes in magnetic-mirror and toridal plasmas were developed [6,7]. By using the azimuthally rotating-field ion cyclotron range of frequencies (ICRF) antannae a few experimental trials have been made to clarify phenomena associated with the RF-induced fluxes in the Phadrus-B, Gamma 10, and small linear devices [8].

Here our goal is to give a physical picture for the generation of test-particle drifts that are perpendicular to background magnetic-field lines in the presence of traveling RF fields with the cyclotron frequencies. On the basis of the single-particle orbit theory, we provide clear-cut interpretations for the drift generation, which may be significant in suggesting a direction to experimental procedures and constructing a kinetic-theoretic description of the interaction between a wave around the cyclotron frequency and a magnetized plasma. The result is also useful for impurity control [9] and helium ash removal [10] in fusion plasmas, ion-species [11] and isotope [12] separations, and electron-orbit control in cyclotron fast-wave tubes such as gyrotrons [13] and peniotrons [14].

In Sec. II, a physical origin of the drift generation is described. A perturbation method and numerical calculations in the orbit theory are presented in Secs. III and IV, respectively. Sections V and VI contain discussions and conclusions, respectively.

II. PHYSICAL ORIGIN

To illustratively clarify the physical mechanism underlying the drift-generation process in the presence of waves traveling perpendicularly to background magnetic-field lines $\mathbf{B}_0$ that are parallel to the z direction (directed out of the page), we consider the motion of an ion of mass m and charge q (>0) in a x-y plane, which gyrates about the magnetic field with the period T or ion cyclotron frequency Ω [$=-(q/m)B_0<0$]. When a simple RF electric field directed in the y direction is present ($E_y=\hat{E}\sin\omega t$; $\hat{E}$ is the amplitude, $\omega/2\pi$ is the frequency), the ion trajectory under the condition of the cyclotron resonance ($\omega=-\Omega$) can easily be obtained from the equation of motion. As shown by arrows in Fig. 1(a), we indicate the instantaneous strength and direction of this RF field on the zeroth-order Larmor orbit in the absence of the RF field, which is a circle starting at a point "0" ($y=-y_0$, $t=0$). Strictly following the upward ("0"→"2") and downward ("2"→"4") ion motion, the E-field direction reverses at every half-cycle (points "0," "2," and "4") and the RF field continuously accelerates the ion to yield an ever increasing Larmor radius, as given on the left-hand side of Fig. 2(b).

Next let us consider the case when the RF field travels

*Present address: Department of Electrical and Electronic Engineering, Ibaraki University, Hitachi 316, Japan.

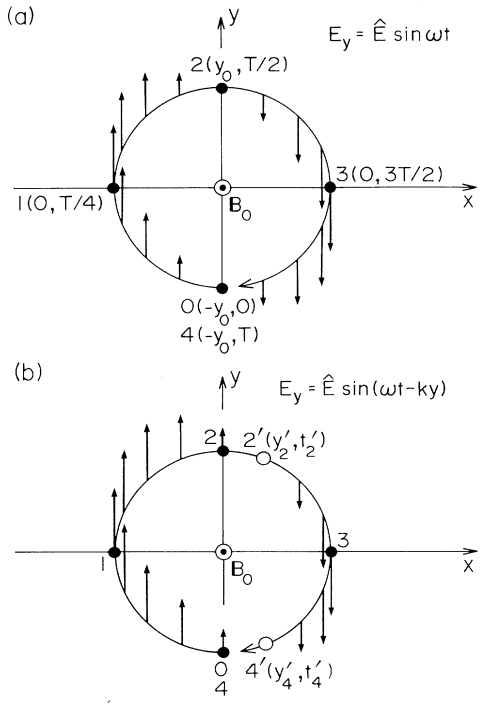

FIG. 1. Vectors of RF electric field E_y at $\omega=-\Omega$, which are indicted on the ion Larmor trajectory (circle) in the absence of the RF field. (a) $k=0$ and (b) $k>0$. The magnetic field is directed out of the page.

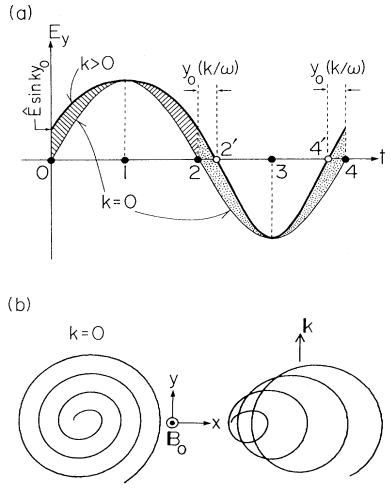

FIG. 2. (a) The RF electric fields at $\omega=-\Omega$ along the ion Larmor trajectory, which are plotted versus time in accordance with Fig. 1. (b) Temporal evolutions of the ion trajectory at $\omega=-\Omega$ for the cases of $k=0$ and $k>0$.

in the y direction [$E_y=\hat{E}\sin(\omega t-ky)$; k is the wave number]. In order to gain an intuitive insight into wave-number effect, k is assumed to be infinitely small ($|ky|\ll 1$). Even under the condition of $\omega=-\Omega$, the resonant relation between the instantaneous ion position and RF field is now collapsed due to a finite phase shift arising from the ky term, as shown in the vicinity of the points "2" ($y=y_0$, $t=T/2$) and "4" ($y=-y_0$, $t=T$) of Fig. 1(b), where a case of $k>0$ is illustrated. To better understand, E_y is plotted as a function of t in Fig. 2(a). Being different from the case of $k=0$ (the cyclotron resonance), a finite RF field that is directed upward is already present at the staring point "0," and the E-field direction reverses at points "2′" ($y=y_2'$, $t=t_2'$) and "4′" ($y=y_4'$, $t=t_4'$) just behind the point "2" and just ahead of the point "4," respectively , while the ion changes its direction at the points "2" and "4" along the zeroth-order orbit. Since the total amount of ion acceleration by the RF field in the left-hand part of the Larmor circle ("0"→"2") is larger than in the right-hand part ("2"→"4"), as is evident from Figs. 1(b) and 2(a), the ion attains a maximum velocity around the position "2" and a minimum velocity around the position "4." Accordingly the curvature of the projection of the trajectory in the upper part ("1"→"3") becomes smaller than in the lower part ("3"→"1"). As a result the circle is converted into an asymmetric curve; in the motion along this curve the projection of the ion is gradually displaced to the right ($x>0$) with its gyroradius increasing, as presented on the right-hand side of Fig. 2(b). This displacement is the traveling-RF-field drift perpendicular both to the wave propagation and background magnetic-field lines, the generation-mechanism explanation of which is similar to that of a dc electric-field drift in a magnetic field [15].

Here we can estimate a difference of times when the RF fields change their directions in Figs. 1 and 2(a). This Δt between the two cases of $k=0$ and $k\neq 0$ is given as follows:

$$\Delta t_2=t_2'-t_2\simeq\frac{y_0}{\omega/k}\ , \tag{1}$$

$$\Delta t_4=t_4'-t_4\simeq-\frac{y_0}{\omega/k}\ , \tag{2}$$

because $\omega t_2=\pi$, $\omega t_2'-ky_2'=\pi$, $y_2'\simeq y_0$, and $\omega t_4=2\pi$, $\omega t_4'-ky_4'=2\pi$, $y_4'\simeq -y_0$, respectively. Thus, the traveling RF field takes longer time by the value of $\Delta t_2-\Delta t_4$ [$\simeq 2y_0/(\omega/k)$=Larmor-diameter/phase velocity] to sweep the particle with a velocity component in the direction of wave propagation ("0"→"2") than to sweep the particle with a velocity component in the opposite direction of wave propagation ("2"→"4"). This difference of acceleration (interaction) time during one Larmor cycle is considered to be the origin of the particle-drift generation. The direction of the drift reverses ($x<0$) when the wave propagates in the opposite direction ($y<0$), and an electron under the influence of RF fields with the electron cyclotron frequency drifts in the opposite direction of the ion drift described above.

III. PERTURBATION METHOD

In this section an orbit theory is developed in order to derive an analytic expression for the drift generation. For simplicity we consider two perpendicular RF electric fields, E_x and E_y, 90° out of phase (revolving in the positive sense in the x-y plane) in the magnetic field, which travel in the y direction with wave number k and ampli-

tudes of $\epsilon_x\hat{E}$ and $\epsilon_y\hat{E}$, respectively:

$$\mathbf{E}_\perp=\epsilon_x\hat{E}\cos(\omega t-ky)\hat{\mathbf{x}}+\epsilon_y\hat{E}\sin(\omega t-ky)\hat{\mathbf{y}}\ . \tag{3}$$

Here $\hat{\mathbf{x}}$ and $\hat{\mathbf{y}}$ are unit vectors in the x and y directions, respectively. From Maxwell's induction equation, the RF magnetic field is given by

$$\frac{\partial B_z}{\partial t}=k\epsilon_x\hat{E}\sin(\omega t-ky)\ . \tag{4}$$

When we define $E_\perp=E_x+iE_y$ and $v_\perp=v_x+iv_y$, the equation of nonrelativistic motion of a charged particle with perpendicular velocity (v_x,v_y) is

$$\frac{dv_\perp}{dt}-i\Omega\left[1+\frac{B_z}{B_0}\right]v_\perp=\frac{q}{m}E_\perp\ , \tag{5}$$

where Ω is the cyclotron frequency (<0 for ions, >0 for electrons). The particle trajectory can generally be obtained by solving the nonlinear differential equation (5) after substituting Eqs. (3) and (4) into Eq. (5). Here we separately treat two cases, $\omega\neq\mp\Omega$ and $\omega=\mp\Omega$ (upper sign for ions; lower sign for electrons).

A. $\omega\neq\mp\Omega$

In the case of $k=0$, Eq. (5) is reduced to a linear differential equation and the trajectory is easily obtained as follows:

$$x=x_0+\alpha\frac{\epsilon_x\omega+\epsilon_y\Omega}{\omega(\omega^2-\Omega^2)}(1-\cos\omega t)-\left[\alpha\frac{\epsilon_x\Omega+\epsilon_y\omega}{\Omega(\omega^2-\Omega^2)}+\frac{v_{y0}}{\Omega}\right](1-\cos\Omega t)+\frac{v_{x0}}{\Omega}\sin\Omega t\ , \tag{6}$$

$$y=y_0-\alpha\frac{\epsilon_x\Omega+\epsilon_y\omega}{\omega(\omega^2-\Omega^2)}\sin\omega t+\frac{v_{x0}}{\Omega}(1-\cos\Omega t)+\left[\alpha\frac{\epsilon_x\Omega+\epsilon_y\omega}{\Omega(\omega^2-\Omega^2)}+\frac{v_{y0}}{\Omega}\right]\sin\Omega t\ , \tag{7}$$

where $\alpha=(q/m)\hat{E}$, and (v_{x0},v_{y0}) and (x_0,y_0) are the initial velocity and position, respectively.

In order to represent the finite-k effect analytically, we apply a perturbation method for solving the nonlinear equation (5). Let us substitute the trajectory for the case of $k=0$ [Eqs. (6) and (7)] into Eqs. (3) and (4) after expanding them in terms of the small parameter $|ky|\ll 1$ (long wavelength or small Larmor radius approximation). Then Eq. (5) is reduced to a linear differential equation, $dv_\perp/dt+p(t)v_\perp=q(t)$ with

$$p(t)\simeq-i\Omega\left[1+\frac{k\epsilon_x\alpha}{\omega\Omega}\cos\omega t\right]\ , \tag{8}$$

$$\begin{aligned}q(t)\simeq&(\epsilon_xK_1+i\epsilon_yK_2)\cos(\omega-\Omega)t+(-\epsilon_xK_2+i\epsilon_yK_1)\sin(\omega-\Omega)t\\&+(\epsilon_x\alpha-i\epsilon_yK_3)\cos\omega t+(\epsilon_xK_3+i\epsilon_y\alpha)\sin\omega t+(-\epsilon_xK_1+i\epsilon_yK_2)\cos(\omega+\Omega)t\\&-(\epsilon_xK_2+i\epsilon_yK_1)\sin(\omega+\Omega)t+\epsilon_xK_4\cos2\omega t+i\epsilon_yK_4\sin2\omega t-\epsilon_xK_4\ ,\end{aligned} \tag{9}$$

where the terms of orders higher than the second in k are neglected, and $K_1=(k\alpha/2\Omega)(v_{y0}+\beta)$, $K_2=k\alpha v_{x0}/2\Omega$, $K_3=k\alpha(y_0+v_{x0}/\Omega)$, $K_4=k\alpha\beta/2\omega$, and $\beta=\alpha(\epsilon_x\Omega+\epsilon_y\omega)(\omega^2-\Omega^2)$. Solving the differential equation, we obtain the particle trajectory in the presence of finite k. Focusing on the frequency range around the cyclotron frequency ($\omega\simeq\mp\Omega$) and picking up the most effective terms [$\propto 1/(\omega\pm\Omega)^2$] with respect to k in the expression of x and y, the trajectory is given by the following equations:

$$\begin{aligned}x\simeq&\alpha\frac{\epsilon_x\omega+\epsilon_y\Omega}{\omega(\omega^2-\Omega^2)}(1-\cos\omega t)-\alpha\frac{\epsilon_x\Omega+\epsilon_y\omega}{\Omega(\omega^2-\Omega^2)}(1-\cos\Omega t)\\&\mp k\alpha^2\frac{(\epsilon_x\Omega+\epsilon_y\omega)[\epsilon_x(2\Omega\pm\omega)+\epsilon_y\omega]}{2\omega^2(\omega\pm\Omega)^2(\omega\mp\Omega)(\omega\pm2\Omega)}\\&\times[1-\cos(\omega\pm\Omega)t]\ ,\end{aligned} \tag{10}$$

$$y\simeq\alpha\frac{\epsilon_x\Omega+\epsilon_y\omega}{\Omega(\omega^2-\Omega^2)}\left[-\frac{\Omega\sin\omega t}{\omega}+\sin\Omega t\right]\ . \tag{11}$$

If we write $\delta=\omega\pm\Omega$, then the above equations can be written as

$$(x-x_d)^2+y^2\simeq\frac{(\epsilon_x\mp\epsilon_y)^2}{\delta^2}\frac{\hat{E}^2}{B_0^2}\sin^2\left[\frac{\delta t}{2}\right]\ , \tag{12}$$

$$x_d=\pm k\frac{(\epsilon_x\mp\epsilon_y)^2}{2\delta^2}\frac{\hat{E}^2}{B_0^2}\sin^2\left[\frac{\delta t}{2}\right]\ . \tag{13}$$

The trajectory described in Eqs. (12) and (13) is a circular gyration whose radius varies sinusoidally at the beat frequency $|\delta|/2\pi$. Due to the finite k effect, in addition, the gyration center is forced to oscillate in the x direction with the beat frequency $|\delta|/2\pi$.

The situation when $\omega=\mp\Omega$ represent a singular case because the solution given by Eqs. (10) and (11) becomes indeterminate. It is therefore necessary to go back to the original equations of motion and re-solve the problem for this case.

B. $\omega=\mp\Omega$

When $\omega=\mp\Omega$ and $k=0$ (this case is called "the cyclotron resonance"), the trajectory is determined by the

same procedure as in the case of Eqs. (6) and (7) in the following equations:

$$x=x_0\pm\frac{\epsilon_y}{\Omega^2}\alpha-\frac{v_{y0}}{\Omega}+\frac{v_{y0}\Omega\mp\epsilon_y\alpha}{\Omega^2}\cos\Omega t+\frac{v_{x0}}{\Omega}\sin\Omega t + \frac{\epsilon_x\mp\epsilon_y}{2\Omega}\alpha t\sin\Omega t \ , \tag{14}$$

$$y=y_0+\frac{v_{x0}}{\Omega}(1-\cos\Omega t)+\frac{2v_{y0}\Omega+(\epsilon_x\mp\epsilon_y)\alpha}{2\Omega^2}\sin\Omega t - \frac{\epsilon_x\mp\epsilon_y}{2\Omega}\alpha t\cos\Omega t \ . \tag{15}$$

Since the secular terms ($\propto t$) become dominant after a sufficient length of time, the orbit is described by $x^2+y^2\simeq[(\epsilon_x\mp\epsilon_y)\alpha t/2\Omega]^2$, which yields an ever-increasing Larmor radius [16].

Here the perturbation method described in Sec. III A is again used to derive the finite k effect. Then $p(t)$ and $q(t)$ in the reduced linear differential equation are given by

$$p(t)\simeq-i\Omega\left[1\mp\frac{k\epsilon_x\alpha}{\Omega^2}\cos\Omega t\right] , \tag{16}$$

$$q(t)\simeq(-\epsilon_xK_1'+i\epsilon_yK_2)+(\epsilon_x\alpha-i\epsilon_yK_3)\cos\Omega t \mp(\epsilon_xK_3+i\epsilon_y\alpha)\sin\Omega t +(\epsilon_xK_1'+i\epsilon_yK_2)\cos2\Omega t\pm(\epsilon_xK_2-i\epsilon_yK_1')\sin2\Omega t +i\epsilon_yK_4't\cos2\Omega t\pm\epsilon_xK_4't\sin2\Omega t+i\epsilon_yK_4't \ , \tag{17}$$

where $K_1'=\pm(k\alpha/2\Omega)[v_{y0}+(\epsilon_x\mp\epsilon_y)\alpha/2\Omega]$, $K_4'=k\alpha^2(\epsilon_x\mp\epsilon_y)/4\Omega$. By solving the differential equation the trajectory, after a sufficient length of time, is obtained as follows:

$$x\simeq\frac{\epsilon_x\mp\epsilon_y}{2\Omega}t(\pm K_3\cos\Omega t+\alpha\sin\Omega t)\pm k\frac{(\epsilon_x\mp\epsilon_y)^2\alpha^2}{8\Omega^2}t^2 \ , \tag{18}$$

$$y\simeq\frac{\epsilon_x\mp\epsilon_y}{2\Omega}t(-\alpha\cos\Omega t\pm K_3\sin\Omega t) \ . \tag{19}$$

Since k is so small that $\alpha\gg K_3$ in our approximation, Eqs. (18) and (19) combine to give

$$(x-x_d)^2+y^2\simeq\frac{(\epsilon_x\mp\epsilon_y)^2\hat{E}^2}{4B_0^2}t^2 \ , \tag{20}$$

$$x_d=\pm k\frac{(\epsilon_x\mp\epsilon_y)^2}{8}\frac{\hat{E}^2}{B_0^2}t^2 \ . \tag{21}$$

Equation (21) originates from the last three secular terms on the right-hand side of Eq. (17) (RF electric field) and the second term on the right-hand side in Eq. (16) (RF magnetic field). Thus, the secular drift in the x direction is found to appear for finite k at $\omega=\mp\Omega$ and is perpendicular to the directions of both background magnetic-field lines and wave propagation. Since the drift appears even for $\epsilon_x=0$ or $\epsilon_y=0$ (linearly polarized wave) in Eq. (21), it is not essential for its generation whether the RF fields revolve or not. When the RF electric field is represented by a scalar potential ($\mathbf{k}\|\mathbf{E}_\perp$) such as electrostatic waves, the secular drift is obtained by eliminating the RF magnetic field B_z in Eq. (5), i.e., the second term in Eq. (16). The result corresponds to Eqs. (20) and (21) for the case of $\epsilon_x=0$.

Here we discuss the case of $\epsilon_x=0$ to provide a more quantitative explanation than in Sec. II for the drift-generation mechanism. Then, the electric field in Eq. (3) is approximated by

$$\mathbf{E}_\perp\simeq\epsilon_y\hat{E}(\mp\sin\Omega t-ky\cos\Omega t)\hat{\mathbf{y}} \ . \tag{22}$$

The second term on the right-hand side is an electric field $\mathbf{E}^{(2)}$ caused by the finite wave number, which is superimposed on the first term determining the trajectories of cyclotron-resonance particles. Here the cyclotron-resonance trajectory is defined to be of the first order. The amplitude of $\mathbf{E}^{(2)}$ is in proportion to the first-order particle displacement along the wave-traveling direction, which is given by $y\simeq\pm(\epsilon_y/2\Omega)\alpha t\cos\Omega t$ in Eq. (15). Then, $\mathbf{E}^{(2)}\simeq\pm k(\epsilon_y^2/4)(\hat{E}^2/B_0)t(1+\cos2\Omega t)\hat{\mathbf{y}}$, i.e., $\mathbf{E}^{(2)}$ with the oscillation frequency $2|\Omega|$, always points in the same direction as $\mathbf{k}$ for ions and in the opposite direction of $\mathbf{k}$ for electrons. In Fig. 3, $\mathbf{F}^{(2)}$ ($=q\mathbf{E}^{(2)}$) is depicted on the first-order ion orbit to illustrate a physical mechanism of the drift generation in this scheme. Thus, in the sense of time average, the particle feels a nonoscillatory force $\bar{\mathbf{F}}^{(2)}$ parallel to the wave-traveling direction. A resultant drift velocity, $(\bar{\mathbf{F}}^{(2)}\times\mathbf{B}_0)/qB_0^2=\pm k(\epsilon_y^2/4)(\hat{E}/B_0)^2t\hat{\mathbf{x}}$, is generated, corresponding to Eq. (21) with $\epsilon_x=0$.

In the case of $\epsilon_y=0$ ($\mathbf{k}\perp\mathbf{E}_\perp$, transverse wave), on the other hand, the RF magnetic field is induced in the z direction and is approximated by $B_z\simeq\pm k\epsilon_x(\hat{E}/\Omega)\cos\Omega t$ in Eq. (4). Since the first-order velocity in the x direction is given by $v_x\simeq(\epsilon_x/2)\alpha t\cos\Omega t$ in Eq. (14), an in-phase component appears in the Lorentz force caused by the finite wave number $\mathbf{F}^{(2)}=q\mathbf{v}_\perp\times\mathbf{B}\simeq\pm qk(\epsilon_x^2/4)(\hat{E}^2/B_0)t(1+\cos2\Omega t)\hat{\mathbf{y}}$. Since the particle feels a nonoscillatory force $\bar{\mathbf{F}}^{(2)}$ parallel to the wave-traveling direction in the sense of the time average, a resultant drift

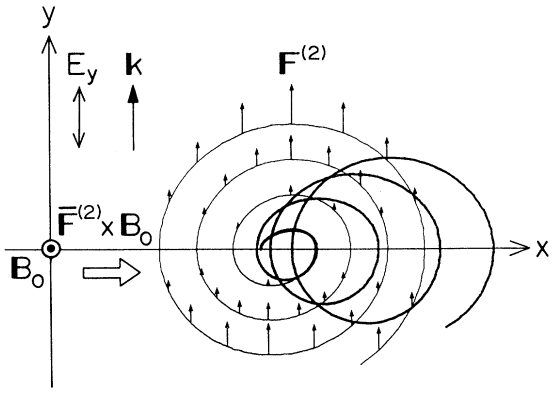

FIG. 3. Schematic for a more quantitative explanation of the ion-drift generation in the case of longitudinal wave ($\omega=-\Omega$). Fine and bold curves denote ion trajectories for $k=0$ and $k\neq0$, respectively.

velocity, $(\bar{\mathbf{F}}^{(2)}\times\mathbf{B}_0)/qB_0^2=\pm k(\epsilon_x^2/4)(\hat{E}/B_0)^2 t\hat{\mathbf{x}}$, is gener- ated, corresponding to Eq. (21) with $\epsilon_y=0$.

IV. NUMERICAL CALCULATIONS

In order to check the prediction described in the previous sections, numerical calculations of ion orbit based on the exact equation of motion in the Cartesian coordinate system are carried out for the longitudinal wave [$\epsilon_x=0$ in Eq. (3)] by the Runge-Kutta-Gill method. In Fig. 4, typical trajectories of a test potassium ion with $v_{x0}=v_{y0}=0$ and $x_0=y_0=0$ are depicted for $\omega=-\Omega$ ($=2\pi\times10^5$ Hz, $B_0=2.57$ kG) and $\hat{E}=0.05$ V/cm. These parameters are determined on the basis of the experimental condition of a Q machine [17], which has been a convenient device for studying basic plasma phenomena. As predicted by Eqs. (20) and (21), the ion drifts in the positive-x direction with its Larmor radius increasing when $k=1.5$ cm^{-1} [Fig. 4(a)] and in the negative-x direction when $k=-1.5$ cm^{-1} [Fig. 4(b)].

We can numerically obtain the gyration-center deviation from the initial position (drift distance x_d) as a function of the square of time or number of Larmor revolutions the ion makes ($\omega t/2\pi$), as presented in Fig. 5, where the analytic solutions [Eq. (21)] are indicated by solid lines. The result in the case of small amplitude ($\hat{E}=0.05$ V/cm: closed circles) agrees well with that of the analytic solution until the considerable number of revolutions. As time goes by, however, a deviation from the analytic solution appears for more earlier time when the amplitude becomes larger ($\hat{E}=0.1$ V/cm: open circles). As the wave number is increased for fixed values of

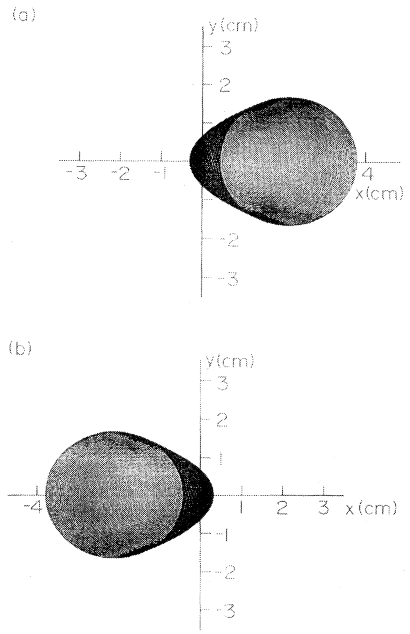

FIG. 4. Numerically calculated trajectories of the potassium ion for the typical values of wave numbers, (a) $k=1.5$ cm^{-1} and (b) $k=-1.5$ cm^{-1}. $\omega=-\Omega=2\pi\times10^5$ Hz, $\hat{E}=0.05$ V/cm, $B_0=2.57$ kG (directed out of the page).

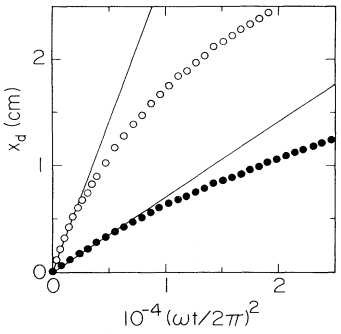

FIG. 5. Dependences of ion-drift distance on the number of Larmor revolutions. Closed and open circles are numerically obtained for $\hat{E}=0.05$ V/cm and 0.1 V/cm, respectively. Results of the analytic solution Eq. (21) are indicated by solid lines. The other parameters are the same as in Fig. 4(a).

$\hat{E}$ ($=0.05$ V/cm) and $\omega t/2\pi$, x_d linearly increases in accordance with the analytic solution (solid line) when the time development is small ($\omega t/2\pi=100$: circles), as shown in Fig. 6. For the larger number of revolutions x_d starts to deviate at a smaller k from the analytic solution and tends to saturate ($\omega t/2\pi=200$: triangles, 350: squares). Dependences of x_d on wave amplitude and background magnetic-field strength are given as a function of the normalized value $(\hat{E}/B_0)^2$ in Fig. 7, where $\hat{E}$ is changed for two values of B_0 ($=2.57$ kG: closed marks, 5.14 kG: open marks). In the case of $\omega t/2\pi=100$ (circles), x_d increases in proportion to $(\hat{E}/B_0)^2$, corresponding to the analytic solution (solid line), while deviations of x_d from it are recognized at smaller $\hat{E}/B_0$ when the number of revolutions becomes larger ($\omega t/2\pi=200$: triangles, 350: squares).

Finally, numerical calculations in the cylindrical coordinate system are carried out from a viewpoint of the application of the principle mentioned above to radial flux control in magnetized plasma column [18]. Here a hypothetical antenna is set at $r_a=3.45$ cm, generating azimuthally traveling fields with mode number m, $E_\theta=\hat{E}\sin(\omega t-m\theta)$, which correspond to the situation

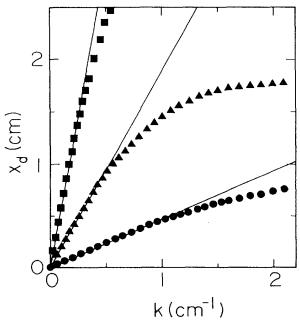

FIG. 6. Ion-drift distance versus wave number. Circles, triangles, and squares are numerically obtained for $\omega t/2\pi=100$, 200, and 350, respectively. Results of the analytic solution Eq. (21) are indicated by solid lines. The other parameters are the same as in Fig. 4(a).

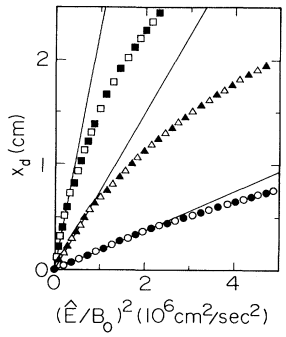

FIG. 7. Dependences of ion-drift distance on RF-field amplitude and background magnetic-field strength. Circles, triangles, and squares are numerically obtained for $\omega t/2\pi=100$, 200, and 350, respectively (t is a value for $\omega/2\pi=10^5$ Hz). Closed and open marks are for $B_0=2.57$ kG ($\omega/2\pi=10^5$ Hz) and 5.14 kG ($\omega/2\pi=2\times10^5$ Hz), respectively. Results of the analytic solution Eq. (21) are indicted by solid lines. The other parameters are the same as in Fig. 4(a).

in Eqs. (3) and (21) with $\epsilon_x=0$. In Fig. 8, typical trajectories of a test potassium ion with the initial speed of 1.1×10^5 cm/sec are depicted for $m=\pm2$, $\hat{E}=1$ V/cm and $\omega=-\Omega$ ($B_0=2.57$ kG). Although the ion starts from the same position, it drifts radially outward and finally collides with the antenna, which is regarded as a wall, in the case of $m>0$, but it drifts inward in the case of $m<0$.

V. DISCUSSIONS

The physical picture of the drift-generation mechanism described in Sec. II is well verified by the perturbation method and numerical calculations in Secs. III and IV, respectively. However, the deviations of the numerical result from the analytic result are found for larger values of $\omega t/2\pi$, k, and $\hat{E}/B_0$ in Figs. 5–7. Since the analytic expression is derived under the condition of long-wavelength approximation, Eq. (21) is valid only when $|ky|\sim|ka|\ll1$, where a is an instantaneous Larmor radius represented by the right-hand side of Eq. (20). Namely, the relation that

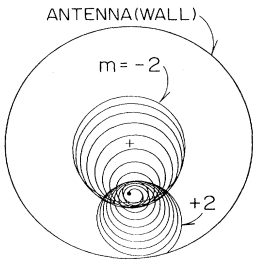

FIG. 8. Numerically calculated ion trajectories at $\omega=-\Omega$ for azimuthal mode number $m=\pm2$. Small closed and large outermost circles denote the initial position and hypothetical antenna diameter ($=6.9$ cm), respectively. $\hat{E}=1$ V/cm, $B_0=2.57$ kG (directed out of the page).

$$|k(\epsilon_x\mp\epsilon_y)|\frac{\hat{E}}{B_0}t\ll1 \tag{23}$$

has to be satisfied in the analytic solution Eq. (21) for the drift. By substituting the critical values of t, k, and $\hat{E}/B_0$, where the deviations start to appear in Figs. 5–7, into the left-hand side of Eq. (23), it is confirmed that the analytic solution can actually be used up to $|ka|\sim1$.

Here let us argue from a viewpoint of momentum transfer from traveling waves. In general, the absorption of RF fields that are excited by an external source in a dissipative medium leads to the generation of momentum flow into the constituent particles and thus to the appearance of a force acting along the wave propagation direction. This dissipative force is given by

$$\mathbf{F}=\sum_{\mathbf{k}}\frac{\mathbf{k}}{\omega(\mathbf{k})}Q(\mathbf{k})\ , \tag{24}$$

where $Q(\mathbf{k})$ is the absorbed wave energy in a unit volume of the medium per unit time and the summation is carried out over all the waves [19]. In our case, on the other hand, the particle velocity in the case of $\omega=\mp\Omega$ and $k=0$ (the cyclotron resonance) is obtained from Eqs. (14) and (15) as follows:

$$v_x\sim\frac{\epsilon_x\mp\epsilon_y}{2}\alpha t\cos\Omega t\ , \tag{25}$$

$$v_y\sim\frac{\epsilon_x\mp\epsilon_y}{2}\alpha t\sin\Omega t\ . \tag{26}$$

Then the power absorbed by the particle is calculated in the following way:

$$Q=\frac{\Delta}{\Delta t}\frac{1}{2}m(v_x^2+v_y^2)\simeq\frac{q^2}{4m}(\epsilon_x\mp\epsilon_y)^2\hat{E}^2t\ . \tag{27}$$

Substituting Eqs. (27) and $\omega=\mp\Omega$ into Eq. (24) gives the particle drift velocity represented by

$$\frac{\mathbf{F}_\perp\times\mathbf{B}_0}{qB_0^2}\simeq\pm k\frac{(\epsilon_x\mp\epsilon_y)^2}{4}\frac{\hat{E}^2}{B_0^2}t\hat{\mathbf{x}}\ , \tag{28}$$

which exactly corresponds to the analytic solution Eq. (21) by the perturbation method in the orbit theory. This argument is also consistent with the plasma kinetic theory on radial transport induced by rotating RF fields [6].

According to our analysis the secular drift of charged particles is generated only when $\omega=\mp\Omega$. However, the consideration described just above means that the drift generation occurs whenever the energy of traveling waves is absorbed by the particles. In magnetized plasmas, on the other hand, the cyclotron damping of waves propagating obliquely to the magnetic field persists in the broad frequency range around the cyclotron frequency. Thus, the plasma particle is expected to drift in the cyclotron range of frequencies.

VI. CONCLUSIONS

In the presence of cyclotron traveling waves with wave-number components perpendicular to background

magnetic-field lines, a test particle is found to be subjected to asymmetric acceleration during one Larmor cycle because it takes a longer time for the waves to sweep the particle with a velocity component in the direction of wave propagation than to sweep the particle with a velocity component in the opposite direction of wave propagation. This asymmetric acceleration leading to a deviation from the cyclotron-resonance trajectory is just the physical origin of the charged-particle drift perpendicular both to the wave propagation and magnetic-field lines. Analytic expressions for the drift generation are obtained by expanding the orbit theory in the long wavelength or small Larmor radius approximation. Numerical calculations demonstrate that the analytic solution is valid up to the condition of $|ka| \sim 1$, where k and a are the wave number and instantaneous Larmor radius, respectively.

According to the principle clarified here, a radially inward or outward drift of charged particles can selectively be controlled by exciting azimuthally traveling waves in a magnetized plasma column. Thus, our result is applicable to flux controls of plasma particles, impurities, helium ash, and isotopes.

ACKNOWLEDGMENTS

The authors are grateful for discussions with T. Hatori, H. Hojo, and T. Watanabe. Discussions with T. Kamimura were helpful for understanding the physical mechanism of the particle drift described.

[1] A. D. MacDonald, *Microwave Breakdown in Gases* (Wiley, New York, 1966); K. Behringer, Plasma Phys. Control. Fusion **33**, 997 (1991); S. Okamura, K. Adati, T. Aoki, D. R. Baker, H. Fujita, H. R. Garner, K. Hattori, S. Hidekuma, T. Kawamoto, R. Kumazawa, Y. Okubo, and T. Sato, Nucl. Fusion **26**, 1491 (1986).

[2] A. G. Litvak, *High-Frequency Plasma Heating* (AIP, New York, 1992); A. E. Costley, U. Gasparino, and W. Kasparek, Nucl. Fusion **33**, 1239 (1993); D. G. Swanson, Phys. Fluids **28**, 2645 (1985); M. Ono, Phys. Fluids B **5**, 241 (1993); G. Taylor and TFTR Group, *ibid.* **5**, 2437 (1993); J.-M. Noterdaeme and G. V. Oost, Plasma Phys. Control. Fusion **35**, 1481 (1993).

[3] Y. Yasaka and R. Itatani, Phys. Rev. Lett. **56**, 2811 (1986); J. R. Ferron, S. N. Golovato, N. Hershkowitz, and R. Goulding, Phys. Fluids **30**, 1869 (1987); S. Tanaka, K. Hanada, H. Tanaka, M. Iida, S. Ide, T. Minami, M. Nakamura, T. Maekawa, and Y. Terumichi, Phys. Fluids B **3**, 2200 (1991); C. K. Phillips and TFTR Group, *ibid.* **4**, 2155 (1992).

[4] D. F. H. Start, N. R. Ainsworth, J. G. Cordey, T. Edlington, W. H. W. Fletcher, M. F. Payne, and T. N. Todd, Phys. Rev. Lett. **48**, 624 (1982); V. V. Alikaev and V. V. Parail, Plasma Phys. Control. Fusion **33**, 1639 (1991).

[5] V. V. Dolgopolov, Fiz. Plazmy **5**, 1203 (1979) [Sov. J. Plasma Phys. **5**, 672 (1979)]; S. Inoue and K. Itoh, in *Plasma Physics and Controlled Nuclear Fusion Research, 1980* (IAEA, Vienna, 1981), Vol. 2, p. 649.

[6] H. Hojo and T. Hatori, J. Phys. Soc. Jpn. **60**, 2510 (1991).

[7] M. Rosenberg, N. A. Krall, and J. B. McBride, Phys. Fluids **28**, 538 (1985); S. Riyopoulos, T. Tajima, T. Hatori, and D. Pfirsch, Nucl. Fusion **26**, 627 (1986).

[8] R. Hatakeyama, N. Hershkowitz, and Phaedrus-B Group, in *Abstracts of the 44th Annual Meeting of the Physical Society of Japan, Hiratsuka, 1989* (Physical Society of Japan, Tokyo, 1989), No. 4, p. 120; M. Inutake, M. Ichimura, Y. Kimura, R. Katsumata, H. Hojo, A. Mase, and S. Miyoshi, in *Abstracts of the 7th Annual Meeting of the Japan Society of Plasma Science and Nuclear Fusion Research, Nagaoka, 1990* (Japan Society of Plasma Science and Nuclear Fusion, Nagoya, 1990), p. 215; N. Y. Sato, T. Tanabe, T. Ikehata, H. Mase, R. Hatakeyama, and N. Sato, in *Proceedings of the 1994 International Conference on Plasma Physics, Foz do Iguacu, Brazil, 1994,* edited by P. H. Sakanaka, E. D. Bosco, and M. V. Alves (INPE, Setor de Eventos, 94 ICPP, São José dos Campos, 1994), Vol. 3, p. 221.

[9] M. Bureš, H. Brinkschulte, J. Jacquinot, K. D. Lawson, A. Kaye, and J. A. Tagle, Plasma Phys. Control. Fusion **30**, 149 (1988); A. Messiaen, *et al.*, *ibid.* **31**, 921 (1989); M. Bureš, J. Jacquinot, K. Lawson, M. Stamp. H. P. Summers, D. A. D'Ippolito, and J. R. Myra, *ibid.* **33**, 937 (1991).

[10] D. L. Hillis *et al.*, J. Nucl. Mater. **196**, 35 (1992); T. Watari, R. Kumazawa, T. Mutoh, T. Seki, K. Nishimura, and F. Shimpo, Nucl. Fusion **33**, 1635 (1993).

[11] T. Sato, K. Matsuura, A. Miyahara, and S. Nagao, J. Phys. Soc. Jpn. **23**, 378 (1967); S. Hidekuma, S. Hiroe, T. Watari, T. Shoji, T. Sato, and K. Takayama, Phys. Rev. Lett. **33**, 1537 (1974).

[12] J. M. Dawson *et al.*, Phys. Rev. Lett. **37**, 1547 (1976); R. Hatakeyama, N. Y. Sato, and N. Sato, Nucl. Instrum. Methods B **70**, 21 (1991); A. I. Karchevskii, V. S. Laz'ko, Yu. A. Muromkin, A. I. Myachikov, V. G. Pashkovskii, A. L. Ustinov, and A. V. Chepkasov, Plasma Phys. Rep. **19**, 214 (1993).

[13] V. A. Flyagin, A. V. Gaponov, M. I. Petelin, and V. K. Yulpatov, IEEE Trans. Microwave Theory Techn. **25**, 514 (1977).

[14] K. Yokoo, H. Shimawaki, X. Wang, N. Sato, and S. Ono, Int. J. Electron. **65**, 619 (1988).

[15] D. V. Sivukhin, in *Reviews of Plasma Physics,* edited by M. A. Leontovich (Consultants Bureau, New York, 1965), Vol. 1, p. 23.

[16] E. H. Holt and R. E. Haskell, *Foundations of Plasma Dynamics* (Macmillan, New York, 1966), p. 201.

[17] R. W. Motley, *Q Machines* (Academic, New York, 1975); N. Sato, H. Sugai, and R. Hatakeyama, Phys. Rev. Lett. **34**, 931 (1975).

[18] R. Hatakeyama, N. Y. Sato, and N. Sato, J. Phys. Soc. Jpn. **60**, 2815 (1991).

[19] A. Bers, in *Plasma Physics,* edited by C. DeWitt and J. Peyraud (Gordon and Breach, New York, 1975), p. 126; V. V. Nemov, Fiz. Plazmy **4**, 1280 (1978) [Sov. J. Plasma Phys. **4**, 714 (1978)].

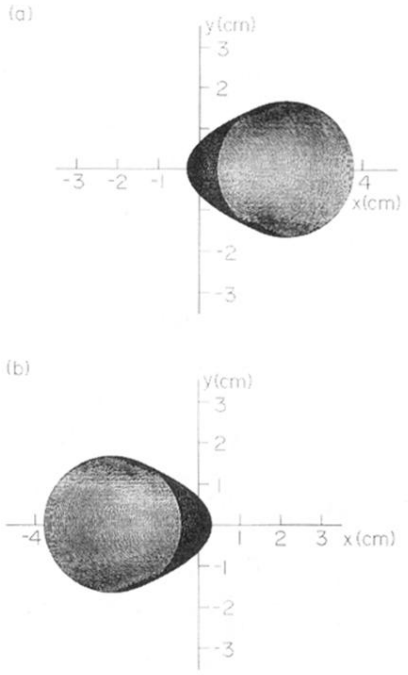

FIG. 4. Numerically calculated trajectories of the potassium ion for the typical values of wave numbers, (a) $k=1.5\ \mathrm{cm}^{-1}$ and (b) $k=-1.5\ \mathrm{cm}^{-1}$. $\omega=-\Omega=2\pi\times10^5$ Hz, $\hat{E}=0.05$ V/cm, $B_0=2.57$ kG (directed out of the page).